DNA Repair 9 (2010) 11–22

Contents lists available at ScienceDirect

DNA Repair

journal homepage: www.elsevier.com/locate/dnarepair

Divergent cellular phenotypes of human and mouse cells lacking the Werner syndrome RecQ helicase

Kiranjit K. Dhillon[a,1], Julia M. Sidorova[b], Tina M. Albertson[b,c], Judith B. Anderson[b], Warren C. Ladiges[d], Peter S. Rabinovitch[b], Bradley D. Preston[b], Raymond J. Monnat Jr.[a,b,*]

[a] Departments of Genome Sciences, University of Washington, Seattle, WA 98195, United States
[b] Departments of Pathology, University of Washington, Seattle, WA 98195, United States
[c] Departments of Pediatrics, University of Washington, Seattle, WA 98195, United States
[d] Departments of Comparative Medicine, University of Washington, Seattle, WA 98195, United States

ARTICLE INFO

Article history:
Received 15 July 2009
Received in revised form
13 September 2009
Accepted 25 September 2009
Available online 5 November 2009

Keywords:
Werner syndrome
RecQ helicase
Mouse model
Progeroid syndrome
Genetic instability

ABSTRACT

Werner syndrome (WS) is a human autosomal recessive genetic instability and cancer predisposition syndrome with features of premature aging. Several genetically determined mouse models of WS have been generated, however, none develops features of premature aging or an elevated risk of neoplasia unless additional genetic perturbations are introduced. In order to determine whether differences in cellular phenotype could explain the discrepant phenotypes of $Wrn^{-/-}$ mice and WRN-deficient humans, we compared the cellular phenotype of newly derived $Wrn^{-/-}$ mouse primary fibroblasts with previous analyses of primary and transformed fibroblasts from WS patients and with newly derived, WRN-depleted human primary fibroblasts. These analyses confirmed previously reported cellular phenotypes of *WRN*-mutant and WRN-deficient human fibroblasts, and demonstrated that the human WRN-deficient cellular phenotype can be detected in cells grown in 5% or in 20% oxygen. In contrast, we did not identify prominent cellular phenotypes present in WRN-deficient human cells in $Wrn^{-/-}$ mouse fibroblasts. Our results indicate that human and mouse fibroblasts have different functional requirements for WRN protein, and that the absence of a strong cellular phenotype may in part explain the failure of $Wrn^{-/-}$ mice to develop an organismal phenotype resembling Werner syndrome.

1. Introduction

Werner syndrome (WS; OMIM 277700) is an autosomal recessive genetic instability and cancer predisposition syndrome that mimics premature aging [1]. WS patients have short stature and develop, beginning in the second decade of life, bilateral cataracts, scleroderma-like skin changes and premature graying and loss of hair. Affected individuals also have an elevated risk of age-associated diseases such as diabetes mellitus, osteoporosis, atherosclerotic cardiovascular disease and cancer. The latter two disease processes are the most common causes of premature morbidity and mortality in WS patients [1,2].

The WS gene *WRN* (also known as *RECQ3* or *RECQL2*) was identified in 1996 by positional cloning. It encodes a member of the evolutionarily conserved human RecQ helicase protein family [3]. WS is an autosomal recessive disease, and cells from WS patients contain *WRN* mutations that lead to the production of truncated, unstable WRN protein that is not appropriately localized to the nucleus [2–5]. For a complete listing of mutations and consequences see 'The Werner Syndrome Locus-Specific Mutational Database': http://www.pathology.washington.edu/research/werner/database/. RecQ loss-of-function mutations have also been found in two other heritable genetic instability-cancer predisposition syndromes: *BLM* mutations are found in Bloom syndrome (BS) patients, and *RecQL4* mutations in a subset of Rothmund-Thomson syndrome (RTS) patients at high risk of developing osteosarcoma [6–8].

All five of the human RecQ helicase proteins share a conserved helicase domain possessing DNA-dependent ATPase and 3′–5′ helicase activities [9–11] (reviewed in [15]). WRN is unique among the human RecQ helicase proteins in possessing an additional 3′–5′ exonuclease activity encoded in an N-terminal domain [12–14]. Purified WRN protein preferentially binds to and unwinds or degrades a number of substrates that mimic DNA metabolic

Abbreviations: CFE, colony-forming efficiency; *cis*-Pt, *cis*-diammineplatinum(II) dichloride; CPT, camptothecin; WS, Werner syndrome; MearF, mouse ear fibroblasts.

* Corresponding author at: Department of Pathology, University of Washington, Box 357705, Seattle, WA 98195-7705, United States. Tel.: +1 206 616 7392; fax: +1 206 543 3967.
E-mail address: monnat@u.washington.edu (R.J. Monnat Jr.).
[1] Present address: Fred Hutchinson Cancer Research Center, Seattle, WA 98109, United States.

1568-7864/$ – see front matter © 2009 Elsevier B.V. All rights reserved.
doi:10.1016/j.dnarep.2009.09.013

intermediates. These include 3- and 4-stranded junctions such as synthetic Holliday junctions, D-loops and T-loops; model replication forks; bubble structures; G4 tetraplexes; and partial DNA duplexes [15]. *In vivo* functional correlates of these WRN biochemical data include defects in homology-dependent recombination resolution [16–18], and a defect in cell cycle progression that may reflect a combination of S/G2 recombination and replication fork progression defects [19].

Several lines of evidence also indicate that telomeres may be an *in vivo* substrate for WRN (reviewed in [20,21]). WRN colocalizes with the telomeric proteins TRF1 and TRF2, and binds to TRF2 and the telomere repeat binding protein POT1 [22–26]. Other proteins that may modulate telomeric functions of WRN include non-homologous DNA end joining proteins such as DNA-PK_{cs}, KU70/80 and DNA ligase IV [27–35], and end or flap processing nucleases such as FEN1 [36–38]. These associations have been shown to modify WRN catalytic activities *in vitro*, and in some instances the ability to process model telomeric repeat or other DNA repair substrates [26,27,39–42]. *In vivo* functional correlates of these protein association data include a telomere lagging strand replication defect in WRN-deficient cells, and karyotypic instability associated with short or undetectable telomeres. Of note, these defects can be suppressed by telomerase expression [20,21,43,44].

WS patient-derived cells and cell lines have a consistent cellular phenotype that can in part be understood in light of the above biochemical and functional data. WRN-deficient cells have reduced cell division potential [45,46]; genomic instability with a mutator phenotype [47,48]; and a distinct form of chromosomal instability referred to as variegated translocation mosaicism [49,50]. WRN-deficient cells are also selectively sensitive to DNA damaging agents such as *cis*-platinum (*cis*-Pt), camptothecin (CPT), and 4-nitroquinoline-1-oxide (4NQO) [51–56].

Several genetically determined mouse models have been developed to analyze how Wrn loss promotes the pathogenesis of WS and associated disease processes. The best-characterized of these models contain either an in-frame deletion of the *Wrn* helicase domain with expression of a truncated protein that retains exonuclease activity ($Wrn^{\Delta hel/\Delta hel}$; [57]), or a *Wrn* null mutation with loss of protein expression ($Wrn^{-/-}$; [58]). Only the latter model faithfully mimics the null mutations found in clinically ascertained WS patients [2–5]. Mouse cells from $Wrn^{\Delta hel/\Delta hel}$ and $Wrn^{-/-}$ mice have discordant phenotypes: $Wrn^{\Delta hel/\Delta hel}$ ES cells are sensitive to camptothecin-induced cell killing, whereas $Wrn^{-/-}/Blm^{+/-}$ MEFs are not [57,58]. Of note, neither mouse model displays premature aging or an elevated risk of tumorigenesis in the absence of additional perturbations. $Wrn^{-/-}$ mutant mice that have been telomerase-deficient for ≥3 generations do develop an age-dependent phenotype resembling WS that includes graying and loss of hair, osteoporosis, kyphosis, cataract formation and tumorigenesis with telomere shortening and karyotypic instability [59–61]. We also showed recently that $Wrn^{-/-}$ mutant mice become hyperinsulinemic and insulin-resistant when fed a high fat diet [62], thus recapitulating the predisposition of WS patients to develop diabetes mellitus [1,2,63,64]. Potential explanations for the discordant cellular and organismal phenotypes of *Wrn*-mutant mice and WS patients include mutation-specific differences; mouse strain-specific effects; and cell type- or species-specific differences. One example of the latter is the strong suppression of mouse – but not human – primary fibroblast proliferation by ambient (20%) oxygen [65,66].

In order to better understand the consequences of WRN loss in mice and men, we systematically compared the cellular phenotypes of primary mouse ear fibroblasts (MearF) from fully backcrossed C57BL/6J $Wrn^{-/-}$ mice with WS patient-derived primary and transformed fibroblasts, and with newly derived, WRN-depleted primary human fibroblasts. Cell proliferation, γ-H2AX phosphorylation, cell survival after DNA damage and cell cycle progression were all quantified after growth in either physiologic (5%) or ambient (20%) O_2. All of these assays had been previously used to identify and characterize the phenotype of WRN-mutant or WRN-depleted human cells (see, *e.g.* [19,67]). Our results demonstrate that WRN loss confers a strong cellular phenotype in early passage human – though not mouse – primary fibroblasts. Our results may explain in part why *Wrn*-mutant mice fail to develop an organismal phenotype that resembles WS, and provide mechanistic clues to the origin of the discrepant cellular phenotypes of Wrn-deficient mice and WRN-deficient humans.

2. Materials and methods

2.1. Chemicals

cis-Platinum (*cis*-Pt), camptothecin (CPT), and bromodeoxyuridine (BrdU) were purchased from Sigma–Aldrich (St. Louis, MO). *cis*-Pt (2 mM) was resuspended in 0.09% NaCl and stored at −20 °C. CPT (1 mM) was resuspended in DMSO and stored at −20 °C. BrdU (10 mM) was resuspended in H_2O and stored protected from light at −20 °C. All chemicals and drugs were diluted to working concentrations just prior to use.

2.2. Mouse breeding and survival analysis

C57BL/6J/129/BALB/c mice harboring a *Wrn* null mutation [58] (kindly provided by Dr. L. Guarente, MIT) were crossed to C57BL/6J mice for >10 generations to create congenic C57BL/6J $Wrn^{+/-}$ mice. Heterozygous $Wrn^{+/-}$ mice were then bred to generate wild type and mutant sib pairs for survival analysis. Mice were multiply housed (1–5 mice per cage) in ventilated Allentown cages (model MBS75JRHMVX) containing Bed-O-Cob (Andersons, Maumee, OH) in a specific pathogen-free (SPF) facility at the University of Washington (Seattle, WA). All studies were conducted with contemporary mutant cohorts and wild type controls housed together in the same room. Food (irradiated Picolab Rodent Diet 20 #5053; PMI Nutrition International, Brentwood, MO) and reverse osmosis water were provided *ad libitum*. All supplies entering animal rooms were autoclaved. Rooms were maintained at 21–23 °C, 45–55% humidity, with 28 air changes/h and a 12 h/12 h light/dark cycle. Sentinel mice were tested quarterly for endo- and ectoparasites, mouse hepatitis virus, mouse parvovirus, and rotavirus and annually for *Mycoplasma pulmonis*, pneumonia virus of mice, reovirus-3, Sendai virus, and Theiler's murine encephalomyelitis virus. All tests were negative. Experimental mice were not tested for *Helicobacter* species or the newly recognized mouse Norovirus.

Genotyping was confirmed twice, using genomic DNA obtained by tail snip at the time of weaning and at sacrifice and the previously published primer pairs pSL3093 × Common.2 and Common.2 × WT.1 [58]. The primer sequences were:

pSL3093: 5′ GCCTGCAGCTGGCGCCAT C 3′,
Common.2: 5′ CAATAACCAATGGAATTCTAAGC 3′
WT.1: 5′ TACATTTGCCATTTTAAGGTGGC 3′.

Mice were monitored daily, and animals were euthanized by CO_2 inhalation when they met one of the following criteria: moribund; visible tumor >1 cm; ulcerating tumor; or dermatitis/self-inflicted wounds that did not respond to treatment with Betadine. Moribund animals were identified on the basis of respiratory distress, decreased activity, or visibly evident loss of body weight. Prism4©software (GraphPad) was used for Kaplan–Meier survival analysis by log–rank comparisons. All pro-

cedures were approved by the University of Washington Animal Care and Use Committee.

2.3. Generation of primary mouse and human fibroblast strains

Mice were sacrificed by CO_2 inhalation at age 6–7 months, and ear tissue was used to generate primary fibroblast strains. Ear tissue was sterilized with Povidone-Iodine swabsticks (PDI, Orangebury, NY), rinsed with 70% ethanol and PBS containing penicillin/streptomycin and 2× Fungizone (Invitrogen, Carlsbad, CA), then minced in PBS containing 1 mg/ml collagenase/dispase (Roche Applied Science, Indianapolis, IN). Tissue fragments were gently rotated at 37 °C in a 5% O_2 incubator for 45 min, then overnight at 37 °C after adding 5 ml of media. Tissue was further dissociated by pipetting, and then filtered through a 100 mm mesh nylon filter (BD Biosciences, San Jose, CA) prior to centrifugation and resuspension in fresh growth media.

New human primary fibroblast cultures were generated from neonatal foreskin tissue by a similar protocol. Tissue was washed in PBS containing penicillin/streptomycin, and then dissociated in PBS supplemented with Dispase II (0.5 g in 7 ml PBS; Roche Applied Science, Indianapolis, IN) for 2 days at 4 °C. The resulting tissue fragments were minced and incubated overnight at 37 °C in media containing 20 mg/ml collagenase type I (Worthington Biochemical, Lakewood, NJ). Cells were collected by centrifugation, resuspended in fresh growth media and divided between two 100 mm plates for growth in 5% O_2 or in 20% O_2.

Mouse and human cells were grown in Dulbecco Modified Eagle's Medium (DMEM) with 4.5 g/L glucose and pyruvate (BioWhittaker, Walkersville, MD), supplemented with 2 mM L-glutamine, 10% (v/v) Fetal Clone III serum (Hyclone, Logan, UT), penicillin G (100 U/ml) and streptomycin sulfate (100 mg/ml; BioWhittaker, Walkersville, MD) and 2× non-essential amino acids (BioWhittaker, Walkersville, MD) in a humidified 37 °C, 7% CO_2 incubator in 5% or 20% O_2. WRN depletion from human fibroblasts was performed and verified by Western blot as previously described [67]. Cell phenotyping assays were performed using early passage mouse ear fibroblasts at population doubling level (PDL) 6–10, or WRN-depleted human fibroblasts at PDL 8–15.

2.4. Cell proliferation and survival analyses

Growth curves were generated for mouse and human primary fibroblast cultures by plating 5000 cells/well in 6-well plates, and performing serial cell counts every 2–3 d. In order to determine survival of MearFs after DNA damage, cells (100, 200 or 500/well) were plated in 6-well plates and allowed to attach overnight prior to treating with *cis*-Pt (1 or 2 μM) or CPT (50 or 100 nM) for 24 h. Cells were then washed once with PBS and fed with complete growth medium lacking drug. Colonies formed after 6–7 d growth were fixed and stained with crystal violet to identify colonies of ≥6 cells to determine colony forming efficiency (CFE) [17,67]. Human fibroblast survival after DNA damage was determined by plating 1.5×10^5 cells in 60 mm plates, allowing attachment overnight, and then treating with *cis*-Pt (1 μM) or CPT (5 or 10 nM) for 24 h in 5% or 20% O_2. Treated cells were then trypsinized and plated (2 or 10 cells/well in 200 μl of growth medium) in the central 60 wells of 96-well plates for growth in 5% or 20% O_2. After 10 d growth, wells were fixed and stained with crystal violet to determine CFE as described above.

Flow cytometric analyses of cell cycle progression were performed using cells that had been labeled with 50 μM BrdU for 2 h, and then harvested either immediately or after additional growth in BrdU-free medium. Labeled cells were fixed with cold 66% ethanol in PBS, and denatured in 2N HCl/0.5% Triton X100 for 30 min prior to neutralization in 100mM Na borate pH 8.5 and resuspension in IFA buffer (10 mM HEPES pH 7.4, 150 mM NaCl, 5% normal goat serum, 0.1% Na azide) supplemented with 0.5% Tween 20. Fixed and denatured cells in IFA buffer were then stained with a mouse anti-BrdU antibody (BD Biosciences, San Jose, CA; 10 μL/10^6 cells) for 1 h at 4 °C prior to staining with an Alexa 488-conjugated anti-mouse secondary antibody (Invitrogen Molecular Probes, Carlsbad, CA) for 1 h at 4 °C in the dark. Immunostained cells were then washed once in IFA/Tween buffer and resuspended in PBS containing 10 μg/mL propidium iodide and 100 μg/mL RNAse A for analysis on an inFlux® flow cytometer (Cytopeia Inc., Seattle, WA). The positions of BrdU-positive and -negative cell populations were determined by comparison with mock-stained, negative control samples that had not been BrdU-labeled. Cells with Alexa 488 fluorescence above the negative control were considered BrdU-positive, and used to determine cell cycle progression as a function of time after labeling. Cell cycle fractions were estimated using FCS Express (De Novo Software, Los Angeles, CA) or M-cycle (Phoenix Flow Systems, San Diego, CA). Data analysis and figures were generated using Summit software (Dako, Carpinteria, CA).

2.5. Flow cytometric analysis of γ-H2AX content

Flow cytometric analysis of γ-H2AX content was performed as previously described with modification [68,69]. In brief, mouse and human primary fibroblasts ($1–2 \times 10^5$ cells) were scrape-harvested, fixed and then immunostained with mouse anti-γ-H2AX primary antibody (Upstate Cell Signaling-JBW301) followed by a goat anti-mouse secondary antibody conjugated with Alexa 488-IgG (Molecular Dynamics A11001) for, respectively, 1 and 2 h. Immunostained cells were then washed and suspended in Tris-buffered saline containing 10 μg/ml propidium iodide for flow cytometry. The position of γ-H2AX-positive cells in flow cytometric profiles was determined by comparison with mock-stained samples that had not been incubated with anti-γ-H2AX antibody. Control MearF and human fibroblasts grown in 5% O_2 were used to define baseline staining to include 1% of the cell population in the positive cell fraction (Gate 1). A second gate included all cells while excluding cell debris (Gate 2). The fraction of cells included in Gate 1 *vs.* Gate 2 was then expressed as the % of γ-H2AX-positive cells above background staining. When comparing multiple cell strains between individuals or within an individual after treatment (e.g., after CPT treatment), the threshold for γ-H2AX-positive cells was established within an experiment by using the control mouse or human Wrn/WRN+ fibroblast culture grown in 5% O_2 that had the lowest absolute staining. This gating was then applied to all samples within an experiment to determine the 'fold' difference in % γ-H2AX-positive cells *versus* the lowest control or an untreated culture.

2.6. Immunofluorescence microscopy of γ-H2AX foci

Immunofluorescence microscopy was performed on cells fixed in 2% paraformaldehyde and permeabilized with cold methanol prior to immunostaining for 1 h each with a mouse monoclonal anti-phosphohistone H2AX (Ser 139) IgG primary antibody (Upstate Cell Signaling-JBW301) followed by a goat anti-mouse secondary antibody conjugated with Alexa 488-IgG (Molecular Probes A11001). Immunostained nuclei were counterstained with DAPI and cells were examined using a Zeiss Axiovert confocal microscope. Digital images were captured at 40× and 63× magnification using the same exposure setting for green fluorescence (γ-H2AX) across all samples within a series to allow a direct comparison of γ-H2AX staining between samples. Images were exported as JPEG files and used with no additional processing other than cropping, with the exception of the three panels displaying $Wrn^{-/-}$ cells in Fig. 8A in which overall image brightness and contrast were

increased uniformly using Adobe Photoshop in order to make the DAPI counterstain more visible.

3. Results

WS patients display premature morbidity and mortality [1,2,64] together with a consistent cellular phenotype in patient-derived fibroblasts: reduced cell proliferation and cell cycle progression defects [45,46]; elevated levels of DNA damage; and sensitivity to killing by DNA damaging agents such as *cis*-Platinum (*cis*-Pt), camptothecin (CPT) and 4-nitroquinoline-1-oxide (4NQO) [51–56]. In order to determine how closely $Wrn^{-/-}$ mouse organismal or cellular phenotypes reflect phenotypes originally defined in WS patients, we determined all-cause mortality of a cohort of $Wrn^{-/-}$ mutant mice and then compared the proliferative behavior, levels of DNA damage and cell survival of primary $Wrn^{-/-}$ fibroblasts with WRN-mutant or -deficient human fibroblasts.

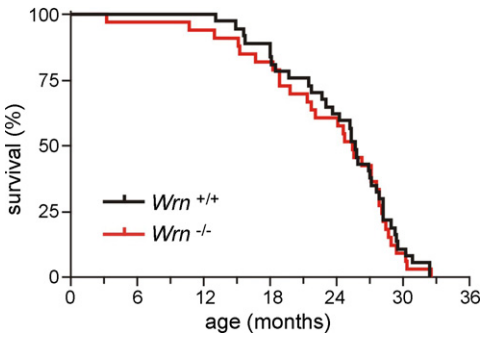

Fig. 1. Survival curves for all-cause mortality of cohorts of $Wrn^{-/-}$ and $Wrn^{+/+}$ mice. Kaplan-Meier survival estimates of *Wrn*-deficient and control mice fully backcrossed onto a C57BL6 strain background. Mice were observed daily until moribund or unexpected natural death (see Section 2). Red line, $Wrn^{-/-}$ ($n = 33$); black line, $Wrn^{+/+}$ ($n = 37$). (For interpretation of the references to color in this figure legend, the reader is referred to the web version of the article.)

3.1. Longevity and tumor incidence in $Wrn^{-/-}$ mutant mice

Previous analyses of *Wrn* mutant mice carrying a null deletion allele ($Wrn^{-/-}$) on a mixed strain background focused on genetic interactions of Wrn loss with additional mutations known to modulate cancer risk or shorten lifespan (see, e.g., *Trp53*, *Blm* and/or *Terc* mutations [58–60]). In order to unambiguously define the organismal consequences of Wrn deficiency alone, we first fully back-crossed $Wrn^{-/-}$ mutant mice [58] onto a C57BL/6J genetic background, and then monitored cohorts of mutant and wild type mice over their natural life span. We observed no significant difference in survival between $Wrn^{-/-}$ and $Wrn^{+/+}$ mice (Fig. 1; $p > 0.05$, log–rank analysis). A high percentage of $Wrn^{-/-}$ and $Wrn^{+/+}$ mice had neoplastic lesions at autopsy, with no difference in tumor incidence or spectrum as a function of genotype (data not shown). The high prevalence of neoplasms in both genotypes likely reflects the common occurrence of neoplasms in aged C57BL/6 mice [70].

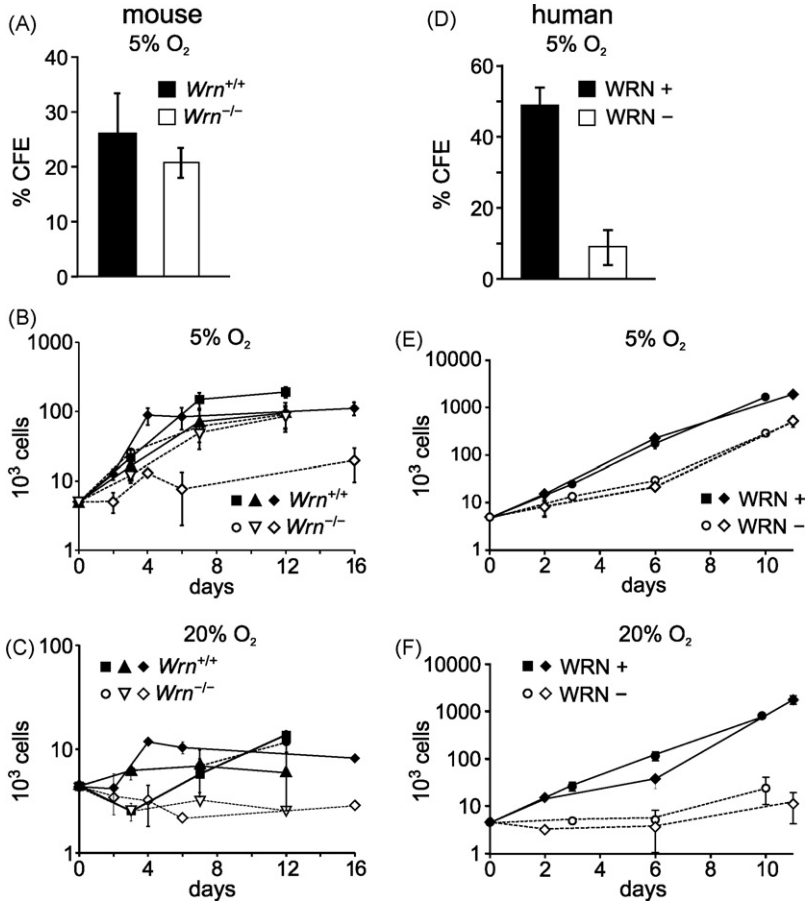

Fig. 2. Proliferation of Wrn/WRN-deficient mouse and human primary fibroblasts. (A and D) Colony forming efficiencies (CFEs) of mouse (A) and human (D) fibroblasts grown in 5% O_2. Data from 3 $Wrn^{+/+}$ and 3 $Wrn^{-/-}$ mouse ear fibroblast strains and two human control or WRN-depleted primary human fibroblasts are shown. (B, C, E and F) Growth curves for the 3 $Wrn^{+/+}$ and 3 $Wrn^{-/-}$ mouse ear fibroblast strains shown in (A), and the 2 WRN-depleted or control human fibroblast strains shown in (B) in either 5% O_2 (B and E) or 20% O_2 (C and F). Error bars in all panels represent standard deviations derived from duplicate samples in the same experiment.

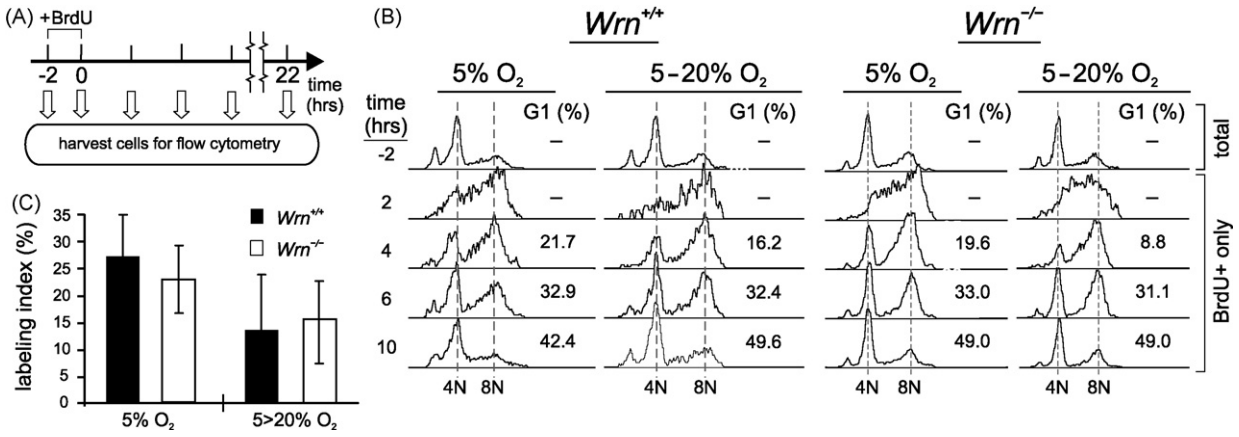

Fig. 3. Cell cycle progression in $Wrn^{+/+}$ and $Wrn^{-/-}$ primary mouse fibroblasts. (A) Experimental design for analyzing cell cycle progression of asynchronous populations of primary mouse fibroblasts (see Section 2 for additional detail). (B) FACS profiles of total cell population (top row, −2 h) and BrdU-labeled sub-populations of $Wrn^{+/+}$ and $Wrn^{-/-}$ mouse ear fibroblasts grown in 5% O_2 or switched to grow in 20% O_2 for 48 h prior to analysis. Two mouse strains with predominantly tetraploid (4N) cell content (see text) as indicated by FACS analysis are shown for easier visual evaluation of profiles. Percent G_1 cells shown to the right of panels were determined using FCS Express software. (C) Average percent BrdU-labeled $Wrn^{+/+}$ and $Wrn^{-/-}$ mouse fibroblasts after 2 h labeling in 5% O_2 or after growth in 20% O_2 for the 48 h prior to analysis. Data from FACS profiles were quantified using FCS Express software using a sample with no BrdU added as a negative control. Error bars indicate standard deviations derived from 2 or 3 independent experiments performed on three independently-derived cell strains for each genotype.

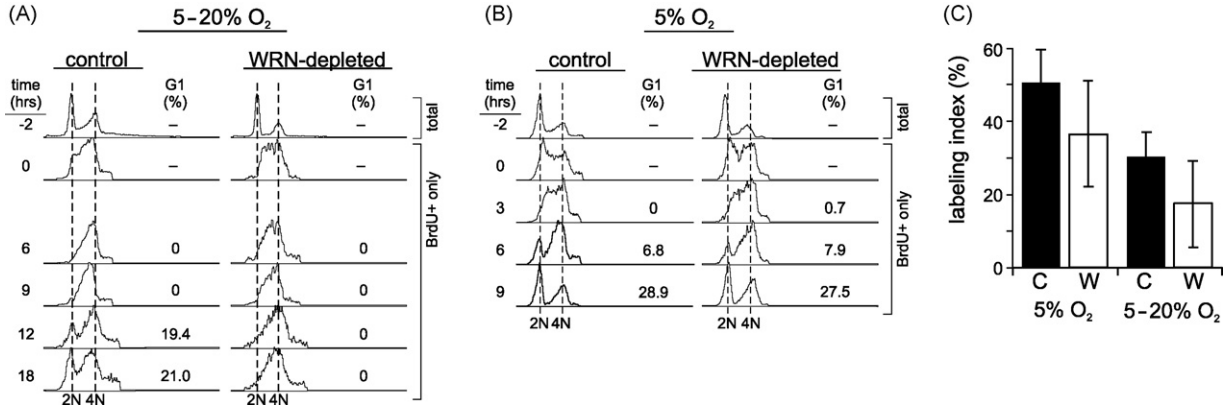

Fig. 4. Cell cycle progression in WRN+ and WRN-depleted primary human fibroblasts. (A and B) FACS profiles of DNA content in total cell population (top row, both panels) and BrdU-labeled sub-populations of control and WRN-depleted primary human dermal fibroblasts switched from 5% to grow in 20% O_2 for 48 h prior to analysis (A), or grown continuously in 5% O_2 (B). G_1 cell fractions were quantified as in Fig. 3B. (C) Average percent BrdU-labeled cells after 2 h of labeling in 5% O_2 or after growth in 20% O_2 for the 48 h prior to analysis. Error bars indicate standard deviations derived from 3 to 5 independent experiments/strain.

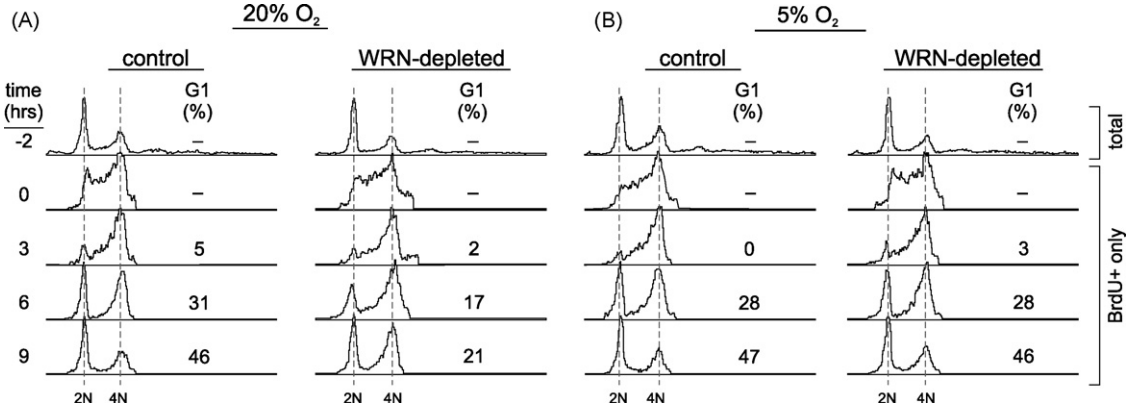

Fig. 5. Human fibroblast strain-specific G_2/M cell cycle progression defect after WRN depletion. (A and B) FACS profiles of total cell population (top row of panels) and BrdU-labeled sub-populations revealed a cell cycle progression defect in one of two newly derived, WRN-depleted primary human dermal fibroblasts. Note the G_2/M delay and reduced G_1 fraction of WRN-depleted, BrdU-labeled cells grown continuously in 20% oxygen at 6 and 9 h timepoints (A). This defect was not observed when the same cells were grown continuously in 5% O_2 (B). G_1 cell fractions were quantified as in Fig. 3B.

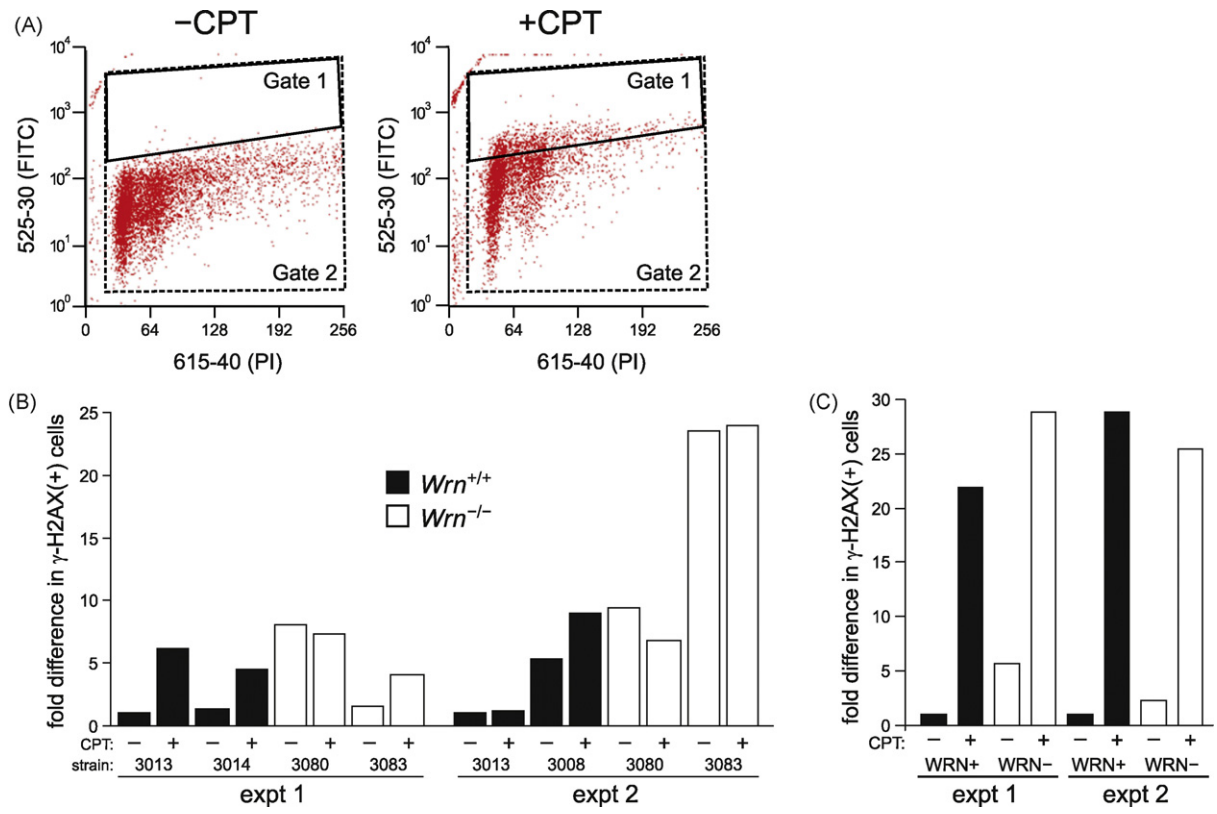

Fig. 6. Spontaneous and induced γ-H2AX formation in mouse and human cells. (A) Example of flow-cytometric profiles of γ-H2AX staining (FITC, 525-530; *Y*-axis) versus DNA content (propidium iodide, 615–640; *X*-axis) of control (WRN+) human fibroblasts prior to and after camptothecin (CPT) treatment. The 'positive staining' gate (Gate 1, see Section 2) was set to include ~1% of cells in control cultures, and then uniformly applied to all samples within an experiment. Gate 2 included all intact cells. CPT, a DNA topoisomerase I inhibitor, was used to induce γ-H2AX staining. (B) Two independent experiments quantifying the fold-difference in γ-H2AX-positive cells in mouse fibroblast strains (2 $Wrn^{+/+}$ and 2 $Wrn^{-/-}$) grown in 5% O_2 ± CPT. $Wrn^{+/+}$ cell strain 3013, grown in 5% O_2 in the absence of CPT, was used to set the 'positive staining' gate (Gate 1; see above and Section 2) to identify and quantify γ-H2AX-positive cells in all samples within an experiment. Cells were treated with 5 μM CPT for 1 h, followed by 1 h recovery prior to staining and analysis. (C) Fold difference in γ-H2AX-positive human control or WRN-depleted fibroblasts in two independent experiments utilizing 1 fibroblast strain grown continuously in 5% O_2 prior to CPT treatment (1 μM CPT for 1 h).

3.2. Generation of new Wrn/WRN-deficient mouse and human primary fibroblast strains

Primary mouse ear fibroblast (MearF) strains generated from 6-mo-old $Wrn^{-/-}$ and $Wrn^{+/+}$ mice were used to determine cellular phenotype. We had previously demonstrated that WRN-depleted and *WRN*-mutant, WS patient-derived fibroblasts have comparably reduced proliferation, altered cell cycle progression profiles, elevated γ-H2AX phosphorylation and DNA damage sensitivity phenotypes [67]. In order to determine if these phenotypes were affected by oxygen tension, we also generated newly derived primary human fibroblast strains in physiologic (5%) or ambient (20%) oxygen. Human and mouse fibroblasts were then assayed after growth in 5% or 20% oxygen or, in some experiments, after transient growth in 20% O_2. WRN-deficient human fibroblasts were generated for these analyses by *WRN*-specific shRNA-mediated WRN

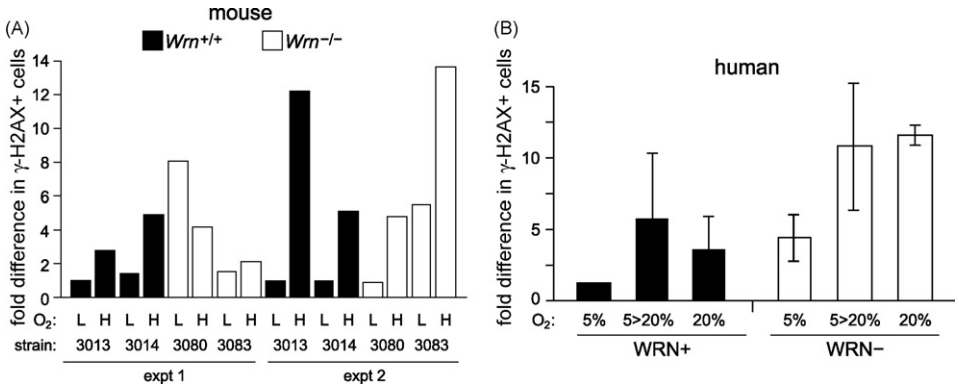

Fig. 7. γ-H2AX levels in mouse and human primary fibroblasts as a function of oxygen tension. (A) The fold-difference in γ-H2AX-positive cells in mouse fibroblast strains (2 $Wrn^{+/+}$ and 2 $Wrn^{-/-}$) grown in 5% O_2 (L), or after 96 h of growth in 20% O_2 prior to analysis (H). Gating and fold-difference calculations were done as described in Fig. 6, panels A and B. (B) Fold-difference in γ-H2AX positive cells in two human fibroblast strains grown in 5% or in 20% O_2, or switched from 5% to grow in 20% O_2 for 96 h prior to analysis. Gating was done as described above for MearF cultures in (Fig. 6A and B). Error bars indicate standard deviations from two (20%) or three (5% and 5% > 20%) independent experiments.

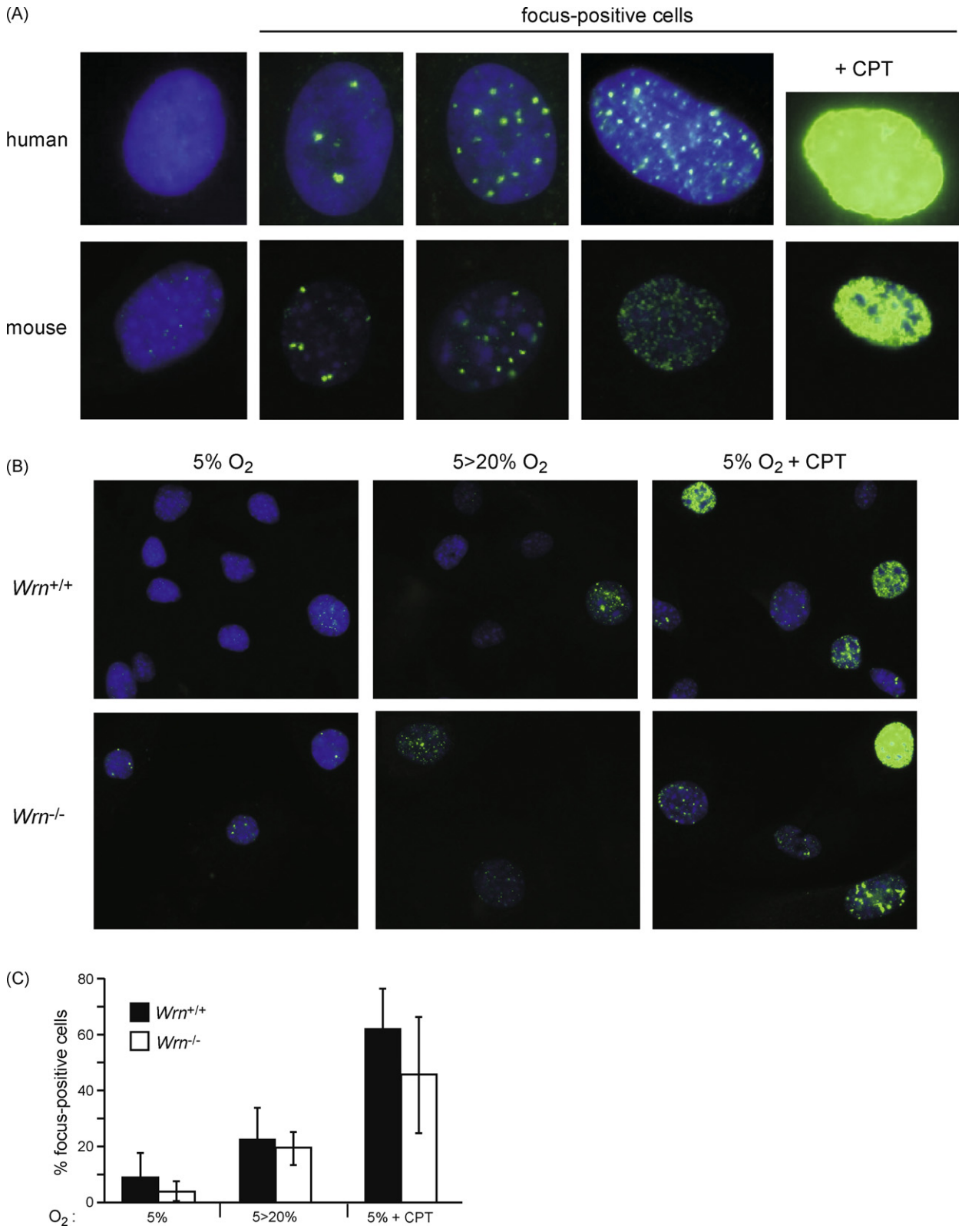

Fig. 8. Induction of γ-H2AX focus formation by oxygen and by camptothecin in mouse and human cells. (A) Examples of γ-H2AX nuclear focus formation in human and mouse fibroblast cultures. The bar above images indicates patterns that were considered focus-positive on the basis of size and number of staining foci. Note that CPT elicited an additional class of very brightly stained mouse and human fibroblasts (+CPT panels). Images of human cells were generated at 63× magnification and mouse cells at 40× magnification. Key: green, γ-H2AX staining; blue, DAPI/DNA counter-staining. (B) Representative examples of γ-H2AX nuclear focus formation in mouse *Wrn*$^{+/+}$ and *Wrn*$^{-/-}$ mouse fibroblasts grown in 5% (left panels), shifted transiently from 5% oxygen to grow in 20% O_2 for 96 h prior to staining (center panels), or after treatment with CPT (5 μM for 1 h) in 5% oxygen (right panels) followed by 1hr recovery prior to immunostaining. Key: green, γ-H2AX staining; blue, DAPI/DNA counter-staining. Note the presence of occasional, intensely stained cells in CPT-treated samples as were observed in (A) +CPT panels. (C) Quantification of focus-positive mouse fibroblasts grown in 5% O_2, switched from 5% to 20% O_2 for 96 h, or treated with CPT as described in (B). Between 120–300 cells were analyzed for each mouse fibroblast strain, in which all types of focus-positive cells shown in (A) were scored. Shown are averages by genotype (2 lines each), with standard deviations.

depletion that was verified by Western blot. Cells with <10% residual WRN protein were used for functional assays.

3.3. Cell proliferation as a function of WRN/Wrn and oxygen tension

We compared the proliferation of 3 independently-derived pairs of $Wrn^{-/-}$ and $Wrn^{+/+}$ MearF strains using as assays colony forming efficiency (CFE) and population-based proliferation [45,67]. Flow cytometric analyses of asynchronous MearF cultures revealed the early emergence of tetraploid cell populations in both $Wrn^{-/-}$ and $Wrn^{+/+}$ cultures that increased with time (data not shown). Thus we used $Wrn^{-/-}$ and $Wrn^{+/+}$ cells of similar passage level and diploid/tetraploid fractions for all analyses. Newly derived $Wrn^{-/-}$ and $Wrn^{+/+}$ MearF strains at population doubling level (PDL) 6–10 had comparable mean CFEs in 5% O_2: 20.9% ($Wrn^{-/-}$) versus 25.9% ($Wrn^{+/+}$; Fig. 2A). Population-based proliferation of the same primary MearF strains revealed mouse-specific, though no genotype-specific, difference in proliferation over 12–16 d in culture (Fig. 2B). MearF strains failed to form cohesive colonies when grown in 20% O_2 (data not shown), and there was comparably strong growth suppression of $Wrn^{-/-}$ and $Wrn^{+/+}$ mouse fibroblasts established in 5% O_2 and then shifted to grow continuously in 20% O_2 (Fig. 2C).

The cellular phenotype of WRN-mutant or deficient human fibroblasts was originally determined using cells grown in 20% O_2 (see above references). In order to determine whether this phenotype was modulated by oxygen tension, we generated and characterized the growth of two independent human dermal fibroblast strains in 5% O_2. WRN depletion from these fibroblasts led to a substantially lower CFE: 8.9% (WRN-depleted) versus 49.2% (isogenic controls; Fig. 2D). In contrast to $Wrn^{-/-}$ mouse fibroblasts, WRN-depleted human fibroblasts grew more slowly than isogenic controls in either 5% and 20% O_2 (compare Fig. 2 panels A–C with D–F). We performed subsequent analyses of mouse and human fibroblasts at 5% O_2 or after transiently shifting from 5% to 20% O_2 in order to compare the behavior of mouse and human cells while minimizing the strong growth-suppressive effect of 20% oxygen on mouse fibroblasts.

3.4. Cell cycle progression as a function of WRN/Wrn and oxygen tension

WRN-depleted human primary fibroblasts grown in 20% O_2 display a late S-G_2/M cell cycle progression delay [19]. In order to determine if this phenotype was present in $Wrn^{-/-}$ mouse fibroblasts, we analyzed cell cycle progression of MearF cells grown continuously at 5% O_2, or transiently in 20% O_2 for 48 h prior to analysis. Cell cycle progression was followed over 22 h using cells that had been labeled with BrdU for 2 h at the beginning of the experiment (Fig. 3A). This approach allowed us to evaluate the rate at which BrdU-labeled S phase cells completed replication and entered a subsequent G_1 phase. The kinetics of S–G_2 progression and transit to a subsequent G_1 phase did not differ between $Wrn^{-/-}$ and $Wrn^{+/+}$ cells. Transient differences were observed between $Wrn^{-/-}$ cells grown in 5% O_2, or in 20% O_2 for 48 h prior to analysis (see, e.g., the 4 h time point in Fig. 3B). However, there was no difference in overall S-G_2 progression as a function of genotype or oxygen tension. Of note, $Wrn^{-/-}$ and $Wrn^{+/+}$ cells had comparable BrdU labeling indices (Fig. 3C).

WRN-depleted primary human fibroblasts grown in 5% O_2 and then shifted to grow in 20% O_2 for 48 hrs prior to analysis displayed a G_2 delay of ≥10 h (Fig. 4A). No corresponding delay was observed in WRN-depleted cells grown continuously in 5% O_2 (Fig. 4B). This difference was not the result of a failure of cells to label with BrdU, as WRN depletion did not significantly suppress the fraction of BrdU-labeled cells (Fig. 4C). These results indicate that transient elevation of oxygen tension can reveal a cell cycle progression defect in WRN-depleted human primary fibroblasts. One of our newly generated primary human fibroblast strains also displayed a late S/G_2 delay after WRN depletion and continuous growth in 20% O_2 (Fig. 5A). This apparent between-individual difference was not observed in cells growth in 5% O_2 (Fig. 5B).

3.5. Role of WRN/Wrn in response to spontaneous and induced DNA damage

We showed previously that WS patient-derived and WRN-depleted human fibroblasts had elevated levels of endogenous DNA damage as indicated by the formation of nuclear foci that contained both co-localizing γ-H2AX [71,72] and phosphoThr68 CHK2 [67]. In order to determine whether $Wrn^{-/-}$ mouse fibroblasts had higher levels of spontaneous DNA damage or an altered response to exogenous DNA damage, we analyzed γ-H2AX content in mouse and human fibroblast cultures as a function of genotype and oxygen tension by two complementary methods, flow cytometry and immunofluorescent microscopy [73].

We used CPT treatment of cells grown at 5% oxygen to induce γ-H2AX formation in order to provide a positive control for flow cytometric analyses (Fig. 6A). Wild type mouse fibroblasts displayed weak (1.1–6-fold) induction of γ-H2AX staining after CPT treatment. $Wrn^{-/-}$ mouse fibroblast strains displayed higher basal levels of γ-H2AX straining than did $Wrn^{+/+}$ fibroblasts, but in 3 of 4 instances failed to demonstrate an increase in γ-H2AX staining after CPT treatment (Fig. 6B). WRN-depleted human fibroblasts also displayed higher basal γ-H2AX staining than did WRN+ controls, but in contrast to $Wrn^{-/-}$ mouse fibroblast strains displayed strong (10–28-fold) and consistent increases in γ-H2AX staining after CPT treatment (Fig. 6C). The lower fold induction of staining in WRN-deficient human fibroblasts reflected the elevated basal γ-H2AX staining in WRN-depleted cells, rather than an attenuated response to CPT treatment (Fig. 6C and additional results not shown).

$Wrn^{+/+}$ mouse fibroblasts grown in 20% oxygen for 96 h prior to analysis displayed consistently higher γ-H2AX staining (2–12-fold) than did $Wrn^{-/-}$ mouse fibroblasts (Fig. 7A). WRN-depleted human fibroblasts displayed higher basal γ-H2AX staining than did WRN+ controls after continuous growth in 5% or in 20% oxygen (Fig. 7B), in agreement with our previous studies [67]. There was no significant difference in γ-H2AX levels in WRN-depleted and control cells shifted transiently from 5% to 20% oxygen, although WRN-depleted cells showed higher levels of induced γ-H2AX staining (Fig. 7B).

The flow cytometric quantitation of γ-H2AX content used above is relatively stringent and most sensitive to large shifts in fluorescence intensity. As flow cytometry alone might miss subtle changes such as increases in the size or nuclear distribution of γ-H2AX foci, we also examined mouse and human fibroblasts by immunofluorescent microscopy in order to determine whether Wrn/WRN loss affected γ-H2AX nuclear focus frequency or distribution. Both mouse and human fibroblasts displayed a range of nuclear γ-H2AX focus staining patterns in which focus number, size and staining intensity varied (Fig. 8A). However, these patterns did not differ between $Wrn^{-/-}$ and $Wrn^{+/+}$ fibroblasts, or in human WRN+ or WRN-depleted cells (Fig. 8A, B and additional results not shown).

CPT treatment of both mouse and human fibroblasts markedly augmented nuclear γ-H2AX focus number and size, and led to the appearance of small numbers of intensely stained cells in both mouse and human cultures (see Fig. 8A, +CPT column). These results parallel what we observed in flow cytometric analyses (Fig. 6). In order to determine whether there was a difference in CPT-induced focus formation in mouse cells as a function of genotype we counted focus-positive cells with two or more large discreet

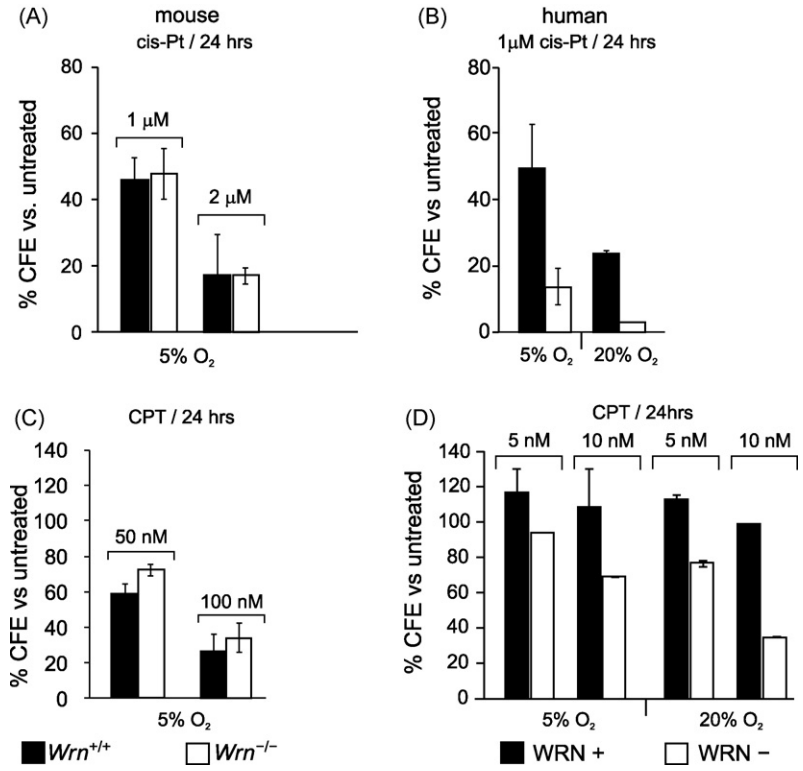

Fig. 9. Survival of mouse and human primary fibroblasts after DNA damage (A and C). Colony-forming efficiencies (CFEs) of 3 $Wrn^{+/+}$ and 3 $Wrn^{-/-}$ mouse primary fibroblast strains grown continuously in 5% O_2 prior to treatment with 1 or 2 μM *cis*-Pt (A) or with 50 or 100 nM CPT for 24 h (C). Survivals are corrected by the CFEs of untreated cells. (B and D) CFEs of control or WRN-depleted primary human fibroblasts grown continuously in 5% or in 20% O_2 prior to treatment with 1 μM *cis*-Pt (B) or with 5 or 10 nM CPT (D) for 24 h. Survivals are corrected by the CFEs of untreated cells in all cases. Error bars indicate standard deviations for duplicate samples of three (mouse) or two (human) fibroblast strains in each experiment.

nuclear foci and/or multiple smaller, bright foci prior to and after CPT treatment (Fig. 8A–C). CPT treatment of mouse cells grown in 5% oxygen resulted in up to 60% focus-positive cells regardless of genotype, compared with 5–10% focus-positive cells in control cultures (Fig. 8C). Focus-positive cells included those with few large foci, and a minority (8–20%) of cells with numerous extremely bright foci (Fig. 8B; 5% + CPT panels).

Transient growth of mouse fibroblasts in 20% oxygen prior to immunofluorescence analysis led to up to 20% focus-positive cells as defined above, though fewer cells with large bright foci than were observed in CPT-treated cells (Fig. 8B, 5–20% panels; Fig. 8C). No significant difference was observed between $Wrn^{-/-}$ and $Wrn^{+/+}$ fibroblasts in the fraction of focus-positive cells after either CPT treatment or growth in 20% oxygen (Fig. 8B, C and additional results not shown). These results indicate that both $Wrn^{-/-}$ and $Wrn^{+/+}$ mouse fibroblasts can form γ-H2AX foci in response to CPT or an acute increase of oxygen tension. The large fraction of CPT-treated mouse fibroblasts that had small numbers of large foci (Fig. 8B) also provides a potential explanation for the low 'fold' induction in γ-H2AX staining that was observed in flow cytometric analyses—these foci raised mean cell staining intensity, though not by enough to push a large fraction of cells over the threshold that had been set to identify γ-H2AX-positive cells (see Fig. 6A).

In summary, mouse and human *Wrn*/WRN-deficient fibroblasts exhibited elevated γ-H2AX staining versus controls when grown in 5% oxygen ± CPT. Mouse and human fibroblasts regardless of WRN genotype also displayed increased γ-H2AX content after transient growth in 20% oxygen. Human fibroblasts depleted of WRN displayed the most genotype-specific difference in which elevated γ-H2AX content was observed after continuous growth in 5%, in 20% oxygen or after CPT treatment using cells grown in 5% oxygen (Figs. 6–8).

3.6. Cell survival after DNA damage

WS patient-derived fibroblasts are selectively killed by several genotoxic agents including DNA cross-linking agents such as *cis*-Pt and topoisomerase I inhibitors such as CPT (see above). In order to determine whether mouse fibroblasts displayed a similar DNA damage sensitivity profile, we treated $Wrn^{-/-}$ or $Wrn^{+/+}$ MearFs grown in 5% O_2 with *cis*-Pt (1 or 2 μM) or with CPT (50 or 100 nM) for 24 h and then determined survival by measuring colony forming efficiency (CFE). We determined in parallel the CFE of CPT-treated, WRN-depleted or control human fibroblasts grown in 5% or 20% O_2. $Wrn^{-/-}$ and $Wrn^{+/+}$ MearFs showed *cis*-Pt or CPT dose-dependent, though not genotype-specific, reductions in CFE after treatment (Fig. 9A and C). In contrast, WRN-depleted human fibroblasts grown in 5% or in 20% O_2 displayed significantly lower CFEs after treatment with *cis*-Pt or with CPT than did control cultures (Fig. 9B and D). The CPT sensitivity we observed in WRN-depleted human cells was comparable to what has been previously reported by us and by others [53,55,74,75].

4. Discussion

The most surprising finding from these analyses was the absence of a strong cellular phenotype in $Wrn^{-/-}$ mouse fibroblasts. We and others had previously noted the strong and consistent cellular phenotype in *WRN*-mutant human fibroblasts and fibroblast cell lines that included reduced cell proliferation, premature cellular senescence, selective DNA damage sensitivity and genetic instability [17,45,47–50,54,67,76,77]. This cellular phenotype is also present in WRN-depleted primary and transformed human fibroblasts, and is accompanied in WRN-depleted primary fibroblasts by an acute DNA damage response (see, *e.g.* [67]). We did not observe

a comparable cellular phenotype in newly derived *Wrn*$^{-/-}$ mouse fibroblasts grown under optimal conditions. This is in contrast to previous reports [57,58,78] where variable cellular phenotypes involving growth or survival were reported.

The absence of a cellular phenotype in *Wrn*-mutant mouse fibroblasts could have several explanations. One potential confounder in these reports was that only one of the genetically determined mouse models of WS [58] utilized a *Wrn* null mutation that leads to the loss of WRN protein as is observed in WS patients [2–5]. We fully back-crossed this *Wrn* null allele into C57BL/6J mice. This provided a genetically homogenous mouse population for these analyses, but may have inadvertently suppressed phenotypes that were present in the original mixed-strain mutant mouse background. This possibility could be further investigated by crossing the *Wrn* null allele into additional mouse strain backgrounds. However, we note that cells and cell lines from WS patients display a strong phenotype regardless of donor genetic background or ethnic origin, and the only suggested genetic background effect on phenotypic expression of human *WRN* null mutations has been for the risk of thyroid carcinoma [79,80].

A second potential explanation for discrepant mouse and human WRN-deficient cellular phenotypes is oxygen tension. The human WRN-deficient cellular phenotype was originally defined using cells grown in 20% (ambient) oxygen (see, *e.g.* [17,45,46,67]). In contrast, mouse fibroblasts grow best at lower oxygen tensions (*e.g.*, 5%; [65,66]). We did not have skin biopsies from WS patients to generate new primary WS fibroblast cultures in 5% oxygen in parallel with the generation of *Wrn*$^{-/-}$ mouse fibroblasts. However, we had shown that the phenotype of *WRN*-mutant and WRN-depleted human primary fibroblasts were very similar [67], and thus compared the phenotypes of newly derived *Wrn*-mutant mouse and WRN-depleted human fibroblasts grown from inception in 5% oxygen. The effect of oxygen tension on cellular phenotype was determined for both mouse and human fibroblasts by either transient (mouse) or continuous (human) growth in 20% as well as 5% oxygen.

Among the cellular phenotypes we examined in WRN-depleted human fibroblasts, only cell cycle progression was affected by oxygen tension. WRN-depleted fibroblasts grown in 20% O_2 displayed a late S-G_2/M cell cycle progression delay [19] that was absent in WRN-depleted cells grown continuously in 5% O_2. This delay could also be revealed in WRN-depleted cells by transient growth in 20% oxygen (Fig. 4A and B). Mouse fibroblasts, in contrast, did not display S-G_2/M progression delay or other cellular phenotypes that were genotype- and oxygen tension-dependent. We did, however, show that shifting mouse and human cells from 5% to grow transiently in 20% oxygen altered cell proliferation and DNA damage measures. These observations are consistent with reports that WRN/Wrn may play a role in the response to oxidative DNA damage at sites including telomeres that may be prone to accumulate oxidative or other forms of DNA damage (see, *e.g.* [81–83]).

The most plausible explanation for the differences in cellular phenotype we observed between Wrn-deficient mouse and WRN-deficient human fibroblasts appears to be a species-specific difference in functional requirements for WRN/Wrn. Short telomeres appear to drive WRN-deficient cellular phenotypes in both human and mouse fibroblasts [43,44,59–61] (reviewed in [20,21]). However, we and others have shown that early-passage human WRN-deficient primary fibroblasts that possess long telomeres already display a strong cellular phenotype. Thus a loss of WRN function at sites *other than* telomeres may be an important driver of cell phenotype in early passage cells. Possible roles for WRN throughout the genome include DNA repair [15], mitotic recombination [16,17], and in the maintenance of *global* replication fork progression rates in response to DNA damage [19]. Loss of these WRN functions would be further accentuated in late-passage cells by progressive telomere shortening [20,21]. This model is consistent with our results, and with the observation that *WRN*-mutant human cells, as well as *Wrn*-mutant/telomerase-deficient mice, develop phenotypes that depend in part on telomere length [20,21,59,60,84,85]. Species-specific differences in the response to DNA damage, at telomeres or other genomic sites, may be a second important determinant of the response to *Wrn*/WRN loss-of-function. We found, for example, that *Wrn*-mutant mouse fibroblasts displayed elevated γ-H2AX staining after transient growth in 20% O_2 or after CPT treatment as do human WRN-deficient fibroblasts, though failed to suppress BrdU labeling or display a cycle progression defect in 20% O_2.

Mechanistic links between the cellular and organismal phenotypes of WS are not well-understood. However, several common 'intermediate' phenotypes including progressive cell loss, reduced cell proliferation, genetic instability and the accumulation of senescent cells *in vivo* are likely to play important roles in the pathogenesis of WS and normal aging [63], as well as the pathogenesis of clinically important, age-associated functional declines and in diseases such as neoplasia [63,86–88]. Despite the absence of a strong cellular or organismal phenotype in Wrn-deficient mice, it should be possible to further investigate links between cellular and organismal functions of Wrn in mice. Precedents for these types of analyses include experiments cited above in which telomere-dependent functions of Wrn could be revealed in later-generation, telomerase-deficient mice with short telomeres [59,60]; experiments that examined the interaction of Wrn deficiency with Tsp53, p21 and PARP-1-deficiency in mice [58,89,90]; and the recent demonstrations that *Wrn*$^{\Delta hel/\Delta hel}$ as well as *Wrn*$^{-/-}$ mutant mice back-crossed into a C57BL/6 strain background become hyperinsulinemic and insulin-resistant when fed a high fat diet [62,83]. Genetic or environmental perturbations that revealed a strong requirement for Wrn/WRN function might identify new ways to modify WS clinical progression, or to suppress or delay the appearance of atherosclerotic cardiovascular disease, diabetes mellitus or cancer. Small molecules or genetic perturbations that revealed a synthetic phenotype with Wrn/WRN loss-of-function might also be useful for selectively killing human tumors that have mutated or silenced *WRN* [91–93].

Conflict of interest

The work reported in our manuscript is original research that has not been published before, and is not under review for publication elsewhere. All of the authors contributed substantially to the manuscript, and all have read and approved the final manuscript for submission. None of the authors has a conflict of interest to declare with regard to this manuscript.

Acknowledgements

We thank Mike Shen and Donna Prunkard for assistance with FACS analyses, Brian Kennedy for use of his confocal microscope and Ranga Venkatesan for help with the flow protocol for γ-H2AX detection. Alden Hackmann provided help with graphics, and Julia Lauper for a careful reading of the ms. This work was supported by NIH grant P01CA77872 to RJM Jr.

References

[1] C.J. Epstein, G.M. Martin, A.L. Schultz, A.G. Motulsky, Werner's syndrome: A review of its symptomatology, natural history, pathologic features, genetics and relationship to the natural aging process, Medicine 45 (1966) 177–221.
[2] M Muftuoglu, J. Oshima, C. von Kobbe, W.H. Cheng, D. Leistritz, V. Bohr, The clinical characteristics of Werner syndrome: molecular and biochemical diagnosis, Human Genet. 124 (2008) 369–377.

[3] C.-E. Yu, J. Oshima, Y.-H. Fu, E.M. Wijsman, F. Hisama, S. Ouais, J. Nakura, T. Miki, G.M. Martin, J. Mulligan, G.D. Schellenberg, Positional cloning of the Werner's syndrome gene, Science 272 (1996) 258–262.
[4] M.J. Moser, J. Oshima, R.J. Monnat Jr., *WRN* mutations in Werner syndrome, Human Mut. 13 (1999) 271–279.
[5] S. Huang, L. Lee, N.B. Hanson, C. Lenaerts, H. Hoehn, M. Poot, C.D. Rubin, D.-F. Chen, C.-C. Yang, H. Juch, T. Dorn, R. Spiegel, E.A. Oral, M. Abid, C. Battista, E. Lucci-Cordisco, G. Neri, E.H. Steed, A. Kidd, W. Isley, D. Showalter, J.L. Vittone, A. Konstantinow, J. Ring, P. Meyer, S.L. Wenger, A.v. Herbay, U. Wollina, M. Schuelke, C.R. Huizenga, D.F. Leistritz, G.M. Martin, I.S. Mian, J. Oshima, The spectrum of *WRN* mutations in Werner syndrome patients, Human Mut. 27 (2006) 558–567.
[6] N.A. Ellis, J. Groden, T.-Z. Ye, J. Straughen, D.J. Lennon, S. Ciocci, M. Proytcheva, J. German, The Bloom's syndrome gene product is homologous to RecQ helicases, Cell 83 (1995) 655–666.
[7] S. Kitao, A. Shimamoto, M. Goto, R.W. Miller, W.A. Smithson, N.M. Lindor, Y. Furuichi, Mutations in *RECQ4L* cause a subset of cases of Rothmund-Thomson syndrome, Nature Genet. 22 (1999) 82–84.
[8] L.L. Wang, A. Gannavarapu, C.A. Kozinetz, M.L. Levy, R.A. Lewis, M.M. Chintagumpala, R. Ruiz-Malanado, J. Contreras-Ruiz, C. Cunniff, R.P. Erickson, D. Lev, M. Rogers, E.H. Zackai, S.E. Plon, Association between osteosarcoma and deleterious mutations in the RECQL4 gene in Rothmund-Thomson syndrome, J. Natl. Cancer Inst. 95 (2003) 669–674.
[9] M.D. Gray, J.-C. Shen, A.S. Kamath-Loeb, A. Blank, B.L. Sopher, G.M. Martin, J. Oshima, L.A. Loeb, The Werner syndrome protein is a DNA helicase, Nature Genet. 17 (1997) 100–103.
[10] N. Suzuki, A. Shimamoto, O. Imamura, J. Kuromitsu, S. Kitao, M. Goto, Y. Furuichi, DNA helicase activity in Werner's syndrome gene product synthesized in a baculovirus system, Nucleic Acids Res. 25 (1997) 2973–2978.
[11] X. Xu, Y. Liu, Dual DNA unwinding activities of the Rothmund-Thomson syndrome protein, RECQ4, EMBO J. 28 (2009) 568–577.
[12] S. Huang, B. Li, M.D. Gray, J. Oshima, I.S. Mian, J. Campisi, The premature aging syndrome protein, WRN, is a 3′ to 5′ exonuclease, Nature Genet. 20 (1998) 114–116.
[13] J.-C. Shen, M.D. Gray, J. Oshima, A.S. Kamath-Loeb, M. Fry, L.A. Loeb, Werner syndrome protein I: DNA helicase and DNA exonuclease reside on the same polypeptide, J. Biol. Chem. 273 (1998) 34139–34144.
[14] J.J. Perry, S.M. Yannone, L.G. Holden, C. Hitomi, A. Asaithamby, S. Han, P.K. Cooper, D.J. Chen, J.A. Tainer, WRN exonuclease structure and molecular mechanism imply an editing role in DNA end processing, Nat. Struct. Mol. Biol. 13 (2006) 414–422.
[15] V.A. Bohr, Rising from the RecQ-age: the role of human RecQ helicases in genome maintenance, Trends Biochem. Sci. 33 (2008) 609–620.
[16] P.R. Prince, M.J. Emond, R.J. Monnat Jr., Loss of Werner syndrome protein function promotes aberrant mitotic recombination, Genes Dev. 15 (2001) 933–938.
[17] Y. Saintigny, K. Makienko, C. Swanson, M.J. Emond, R.J. Monnat Jr., Homologous recombination resolution defect in Werner syndrome, Mol. Cell. Biol. 22 (2002) 6971–6978.
[18] C. Swanson, Y. Saintigny, M.J. Emond, R.J. Monnat Jr., The Werner syndrome protein has separable recombination and viability functions, DNA Repair 3 (2004) 1–10.
[19] J.M. Sidorova, N. Li, A. Folch, R.J. Monnat Jr., The RecQ helicase WRN is required for normal replication fork progression after DNA damage or replication fork arrest, Cell Cycle 7 (2008) 796–807.
[20] A.S. Multani, S. Chang, WRN at telomeres: implications for aging and cancer, J. Cell Sci. 120 (2007) 713–721.
[21] P.L. Opresko, Telomere ResQue and preservation—roles for the Werner syndrome protein and other RecQ helicases, Mech. Ageing Dev. 129 (2008) 79–90.
[22] F.B. Johnson, R.A. Marciniak, M. McVey, W.C. Hahn, L. Guarante, The *Saccharomyces cerevisiae* WRN homolog Sgs1p participates in telomere maintenance in cells lacking telomerase, EMBO J. 20 (2001) 905–913.
[23] P.L. Opresko, C. von Kobbe, J.P. Laine, J. Harrigan, I.D. Hickson, V.A. Bohr, Telomere-binding Protein TRF2 Binds to and Stimulates the Werner and Bloom Syndrome Helicases, J. Biol. Chem. 277 (2002) 41110–41119.
[24] P.L. Opresko, P.A. Mason, E.R. Podell, M. Lei, I.D. Hickson, T.R. Cech, V.A. Bohr, POT1 Stimulates RecQ Helicases WRN and BLM to Unwind Telomeric DNA Substrates, J. Biol. Chem. 280 (2005) 32069–32080.
[25] G. Sowd, M. Lei, P.L. Opresko, Mechanism and substrate specificity of telomeric protein POT1 stimulation of the Werner syndrome helicase, Nucl. Acids Res. 36 (2008) 4242–4256.
[26] B. Ahn, J.W. Lee, H. Jung, G. Beck, V.A. Bohr, Mechanism of Werner DNA helicase: POT1 and RPA stimulates WRN to unwind beyond gaps in the translocating strand, PLoS ONE 4 (2009) e4673.
[27] M.P. Cooper, A. Machwe, D.K. Orren, R.M. Brosh Jr., D. Ramsden, V.A. Bohr, Ku complex interacts with and stimulates the Werner protein, Genes Dev. 14 (2000) 907–912.
[28] B. Li, L. Comai, Functional interaction between Ku and the Werner syndrome protein in DNA end processing, J. Biol. Chem. 275 (2000) 28349–28352.
[29] B. Li, L. Comai, Requirements for the nucleolytic processing of DNA ends by the Werner syndrome protein-Ku70/80 complex, J. Biol. Chem. 276 (2001) 9896–9902.
[30] S.M. Yannone, S. Roy, D.W. Chan, M.B. Murphy, S. Huang, J. Campisi, D.J. Chen, Werner syndrome protein is regulated and phosphorylated by DNA-dependent protein kinase, J. Biol. Chem. 276 (2001) 38242–38248.
[31] B. Li, L. Comai, Displacement of DNA-PKcs from DNA ends by the Werner syndrome protein, Nucl. Acids Res. 30 (2002) 3653–3661.
[32] P. Karmakar, C.M. Snowden, D.A. Ramsden, V.A. Bohr, Ku heterodimer binds to both ends of the Werner protein and functional interaction occurs at the Werner N-terminus, Nucl. Acids Res. 30 (2002) 3583–3591.
[33] P. Karmakar, J. Piotrowski, R.M. Brosh Jr., J.A. Sommers, S.P. Miller, W.H. Cheng, C.M. Snowden, D.A. Ramsden, V.A. Bohr, Werner protein is a target of DNA-dependent protein kinase in vivo and in vitro, and its catalytic activities are regulated by phosphorylation, J. Biol. Chem. 277 (2002) 18291–18302.
[34] B. Li, S. Navarro, N. Kasahara, L. Comai, Identification and biochemical characterization of a Werner's syndrome Protein complex with Ku70/80 and poly(ADP-ribose) polymerase-1, J. Biol. Chem. 279 (2004) 13659–13667.
[35] R. Kusumoto, L. Dawut, C. Marchetti, J. Wan Lee, A. Vindigni, D. Ramsden, V.A. Bohr, Werner protein cooperates with the XRCC4-DNA ligase IV complex in end-processing, Biochemistry 47 (2008) 7548–7556.
[36] R.M. Brosh Jr., C. von Kobbe, J.A. Sommers, P. Karmarkar, P.L. Opresko, J. Piotrowski, I. Dianova, G.L. Dianov, V.A. Bohr, Werner syndrome protein interacts with human flap endonuclease 1 and stimulates its cleavage activity, EMBO J. 20 (2001) 5791–5801.
[37] M. Robert, H.C. Driscoll, G.L. Dianov, J.A. Sommers, Biochemical characterization of the WRN/FEN-1 functional interaction, Biochemistry 41 (2002) 12204–12216.
[38] A. Saharia, L. Guittat, S. Crocker, A. Lim, M. Steffen, S. Kulkarni, S.A. Stewart, Flap endonuclease 1 contributes to telomere stability, Curr. Biol. 18 (2008) 496–500.
[39] D.K. Orren, S. Theodore, A. Machwe, The Werner syndrome helicase/exonuclease (WRN) disrupts and degrades D-loops in vitro, Biochemistry 41 (2002) 13483–13488.
[40] A. Machwe, L. Xiao, D.K. Orren, TRF2 recruits the Werner syndrome (WRN) exonuclease for processing of telomeric DNA, Oncogene 8 (2004) 149-156.
[41] P.L. Opresko, M. Otterlei, J. Graakjaer, P. Bruheim, L. Dawut, S. Kolvraa, A. May, M.M. Seidman, V.A. Bohr, The Werner syndrome helicase and exonuclease cooperate to resolve telomeric D loops in a manner regulated by TRF1 and TRF2, Mol. Cell 14 (2004) 763–774.
[42] P.L. Opresko, P.A. Mason, E.R. Podell, M. Lei, I.D. Hickson, T.R. Cech, V.A. Bohr, POT1 stimulates RecQ helicases WRN and BLM to unwind telomeric DNA substrates, J. Biol. Chem. 280 (2005) 32069–32080.
[43] L. Crabbe, R.E. Verdun, C.I. Haggblom, J. Karlseder, Defective telomere lagging strand synthesis in cells lacking WRN helicase activity, Science 306 (2004) 1951–1953.
[44] L. Crabbe, A. Jauch, C.M. Naeger, H. Holtgreve-Grez, J. Karlseder, Telomere dysfunction as a cause of genomic instability in Werner syndrome, Proc. Natl. Acad. Sci. U.S.A. 104 (2007) 2205–2210.
[45] G.M. Martin, C.A. Sprague, C.J. Epstein, Replicative life-span of cultivated human cells. Effects of donor's age, tissue, and genotype, Lab. Invest. 23 (1970) 86–92.
[46] D. Salk, E. Bryant, K. Au, H. Hoehn, G.M. Martin, Systematic growth studies, cocultivation, and cell hybridization studies of Werner syndrome cultured skin fibroblasts, Human Genet. 58 (1981) 310–316.
[47] K. Fukuchi, G.M. Martin, R.J. Monnat Jr., Mutator phenotype of Werner syndrome is characterized by extensive deletions, Proc. Natl. Acad. Sci. U.S.A. 86 (1989) 5893–5897.
[48] K. Fukuchi, K. Tanaka, Y. Kumahara, K. Marumo, M.B. Pride, G.M. Martin, R.J. Monnat Jr., Increased frequency of 6-thioguanine-resistant peripheral blood lymphocytes in Werner syndrome patients, Human Genet. 84 (1990) 249–252.
[49] H. Hoehn, E.M. Bryant, K. Au, T.H. Norwood, H. Boman, G.M. Martin, Variegated translocation mosaicism in human skin fibroblast cultures, Cytogenet. Cell Genet. 15 (1975) 282–298.
[50] R. Melcher, R. von Golitschek, C. Steinlein, D. Schindler, H. Neitzel, K. Kainer, M. Schmid, H. Hoehn, Spectral karyotyping of Werner syndrome fibroblast cultures, Cytogenet. Cell Genet. 91 (2000) 180–185.
[51] E. Gebhart, R. Bauer, U. Raub, M. Schinzel, K.W. Ruprecht, J.B. Jonas, Spontaneous and induced chromosomal instability in Werner syndrome, Human Genet. 80 (1988) 135–139.
[52] C.E. Ogburn, J. Oshima, M. Poot, R. Chen, K.E. Hunt, K.A. Gollahon, P.S. Rabinovitch, G.M. Martin, An apoptosis-inducing genotoxin differentiates heterozygotic carriers for Werner helicase mutations from wild-type and homozygous mutants, Human Genet. 101 (1997) 121–125.
[53] M. Poot, K.A. Gollahon, P.S. Rabinovitch, Werner syndrome lymphoblastoid cells are sensitive to camptothecin-induced apoptosis in S-phase, Human Genet. 104 (1999) 10–14.
[54] P.R. Prince, C.E. Ogburn, M.J. Moser, M.J. Emond, G.M. Martin, R.J. Monnat Jr., Cell fusion corrects the 4-nitroquinoline 1-oxide sensitivity of Werner syndrome fibroblast cell lines, Human Genet. 105 (1999) 132–138.
[55] P. Pichierri, A. Franchitto, P. Mosesso, F. Palitti, Werner's syndrome cell lines are hypersensitive to camptothecin-induced chromosomal damage, Mutat. Res. 456 (2000) 45–57.
[56] M. Poot, J.S. Yom, S.H. Whang, J.T. Kato, K.A. Gollahon, P.S. Rabinovitch, Werner syndrome cells are sensitive to DNA cross-linking drugs, FASEB J. 15 (2001) 1224–1226.
[57] M. Lebel, P. Leder, A deletion within the murine Werner syndrome helicase induces sensitivity to inhibitors of topoisomerase and loss of cellular proliferative capacity, Proc. Natl. Acad. Sci. U.S.A. 95 (1998) 13097–13102.
[58] D.B. Lombard, C. Beard, B. Johnson, R.A. Marciniak, J. Dausman, R. Bronson, J.E. Buhlmann, R. Lipman, R. Curry, A. Sharpe, R. Jaenisch, L. Guarante, Mutations in the *WRN* gene in mice accelerate mortality in a p53-null background, Mol. Cell Biol. 20 (2000) 3286–3291.
[59] S. Chang, A.S. Multani, N.G. Cabrera, M.L. Naylor, P. Laud, D. Lombard, S. Pathak, L. Guarente, R.A. DePinho, Essential role of limiting telomeres in the pathogenesis of Werner syndrome, Nat. Genet. 36 (2004) 877–882.

[60] X. Du, J. Shen, N. Kugan, E.E. Furth, D.B. Lombard, C. Cheung, S. Pak, G. Luo, R.J. Pignolo, R.A. DePinho, L. Guarente, F.B. Johnson, Telomere shortening exposes functions for the mouse Werner and bloom syndrome genes, Mol. Cell Biol. 24 (2004) 8437–8446.
[61] P.R. Laud, A.S. Multani, S.M. Bailey, L. Wu, J. Ma, C. Kingsley, M. Lebel, S. Pathak, R.A. DePinho, S. Chang, Elevated telomere-telomere recombination in WRN-deficient, telomere dysfunctional cells promotes escape from senescence and engagement of the ALT pathway, Genes Dev. 19 (2005) 2560–2570.
[62] G. Moore, S. Knoblaugh, K.A. Gollahon, P.S. Rabinovitch, W.C. Ladiges, Hyperinsulinemia and insulin resistant in Wrn null mice fed a diabetogenic diet, Mech. Ageing Dev. 129 (2008) 201–206.
[63] B.A. Kudlow, B.K. Kennedy, R.J. Monnat, Werner and Hutchinson-Gilford progeria syndromes: mechanistic basis of human progeroid diseases, Nat. Rev. Mol. Cell. Biol. 8 (2007) 394–404.
[64] M. Goto, Clinical characteristics of Werner syndrome and other premature aging syndromes: pattern of aging in progeroid syndromes, Gann. Monograph. Cancer Res. 49 (2001) 27–39.
[65] S. Parrinello, E. Samper, A. Krtolica, J. Goldstein, S. Melov, J. Campisi, Oxygen sensitivity severely limits the replicative lifespan of murine fibroblasts, Nat. Cell Biol. 5 (2003) 741–747.
[66] R. Di Micco, A. Cicalese, M. Fumagali, M. Dobreva, A. Verrechia, P.G. Pelicci, F. d'Adda di Fagagna, DNA damage response activation in mouse embryonic fibroblasts undergoing replicative senescence and following spontaneous immortalization, Cell Cycle 7 (2008) 3601–3606.
[67] K.K. Dhillon, J. Sidorova, Y. Saintigny, M. Poot, K. Gollahon, P.S. Rabinovitch, R.J. Monnat, Functional role of the Werner syndrome RecQ helicase in human fibroblasts, Aging Cell 6 (2007) 53–61.
[68] P.L. Olive, Detection of DNA damage in inidividual cells by analysis of histone H2AX phosphorylation, Methods Cell Biol. (New York) 75 (2004) 355–373.
[69] R.N. Venkatesan, P.M. Treuting, E.D. Fuller, R.E. Goldsby, T.H. Norwood, T.A. Gooley, W.C. Ladiges, B.D. Preston, L.A. Loeb, Mutation at the polymerase active site of mouse DNA polymerase {delta} increases genomic instability and accelerates tumorigenesis, Mol. Cell Biol. 27 (2007) 7669–7682.
[70] B.N. Blackwell, T.J. Bucci, R.W. Hart, A. Turturro, Longevity, body weight and neoplasia in ad-libitum-fed and diet-restricted C57BL6 mice fed NIH-31 open formula diet, Toxicol. Pathol. 23 (1995) 570–582.
[71] E.P Rogakou, D.R. Pilch, A.H. Orr, V.S. Ivanova, W.M. Bonner, DNA double-stranded breaks induce histone H2AX phosphorylation on serine 139, J. Biol. Chem. 273 (1998) 5858–5868.
[72] T.T. Paull, E.P. Rogakou, V. Yamazaki, C.U. Kirchgessner, M. Gellert, W.M. Bonner, A critical role for histone H2AX in recruitment of repair factors to nuclear foci after DNA damage, Curr. Biol. 10 (2000) 886–895.
[73] Y. Pommier, Topoisomerase I inhibitors: camptothecins and beyond, Nat. Rev. Cancer 6 (2006) 789–802.
[74] P. Pichierri, A. Franchitto, P. Mosesso, F. Palitti, Werner's syndrome protein is required for correct recovery after replication arrest and DNA damage induced in S-phase of cell cycle, Mol. Biol. Cell 12 (2001) 2412–2421.
[75] J. Lowe, A. Sheerin, K. Jennert-Burston, D. Burton, E.L. Ostler, J. Bird, M.H. Green, R.G.A. Faragher, Camptothecin sensitivity of Werner syndrome fibroblasts as assessed by the COMET technique, Ann. N.Y. Acad. Sci. 1019 (2004) 256–259.
[76] D. Salk, K. Au, H. Hoehn, G.M. Martin, Cytogenetic aspects of Werner syndrome, Adv. Exp. Med. Biol. 190 (1985) 541–546.
[77] M.I. Melaragno, D. Pagni, M.d.C. Smith, Cytogenetic aspects of Werner's syndrome lymphocyte cultures, Mech. Ageing Dev. 78 (1995) 117–122.
[78] L. Wang, C.E. Ogburn, C.B. Ware, W.C. Ladiges, H. Youssoufian, G.M. Martin, J. Oshima, Cellular Werner phenotypes in mice expressing a putative dominant-negative human *WRN* gene, Genetics 154 (2000) 357–362.
[79] Y. Ishikawa, H. Sugano, T. Matsumoto, Y. Furuichi, R.W. Miller, M. Gossen, Unusual features of thyroid carcinomas in Japanese patients with Werner syndrome and possible genotype-phenotype relations to cell type and race, Cancer 85 (1999) 1345–1352.
[80] R.J. Monnat Jr., Unusual features of thyroid carcinomas in Japanese patients with Werner syndrome and possible genotype-phenotype relations to cell type and race, Cancer 86 (1999) 728–729.
[81] C. von Kobbe, J.A. Harrigan, A. May, P.L. Opresko, L. Dawut, W.H. Cheng, V.A. Bohr, Central role for the Werner syndrome protein/poly(ADP-ribose) polymerase 1 complex in the poly(ADP-Ribosyl)ation pathway after DNA damage, Mol. Cell. Biol. 23 (2003) 8601–8613.
[82] A.M. Szekely, F. Bleichert, A. Numann, S. Van Komen, E. Manasanch, A. Ben Nasr, A. Canaan, S.M. Weissman, Werner protein protects nonproliferating cells from oxidative DNA damage, Mol. Cell. Biol. 25 (2005) 10492–10506.
[83] L. Massip, C. Garand, R.V.N. Turaga, F. DeschWnes, E. Thorin, M. Lebel, Increased insulin, triglycerides, reactive oxygen species, and cardiac fibrosis in mice with a mutation in the helicase domain of the Werner syndrome gene homologue, Exp. Gerontol. 41 (2006) 157–168.
[84] M.S. Eller, X. Liao, S. Liu, K. Hanna, H. Bäckvall, P.L. Opresko, V.A. Bohr, B.A. Gilchrest, A role for WRN in telomere-based DNA damage responses, Proc. Natl. Acad. Sci. U.S.A. 103 (2006) 15073–15078.
[85] E. Michishita, R.A. McCord, E. Berber, M. Kioi, H. Padilla-Nash, M. Damian, P. Cheung, R. Kusumoto, T.L.A. Kawahara, J.C. Barrett, H.Y. Chang, V.A. Bohr, T. Ried, O. Gozani, K.F. Chua, SIRT6 is a histone H3 lysine 9 deacetylase that modulates telomeric chromatin, Nature 452 (2008) 492–496.
[86] J.R. Mitchell, J.H. Hoeijmakers, L.J. Niedernhofer, Divide and conquer: nucleotide excision repair battles cancer and ageing, Curr. Opin. Cell Biol. 15 (2003) 232–240.
[87] H. de Waard, J. de Wit, T.G.M.F. Gorgels, G. van den Aardweg, J.O. Andressoo, M. Vermeij, H. van Steeg, J.H.J. Hoeijmakers, G.T.J. van der Horst, Cell type-specific hypersensitivity to oxidative damage in CSB and XPA mice, DNA Repair 2 (2003) 13–25.
[88] G.A. Garinis, G.T.J. van der Horst, J. Vijg, H.J. Hoeijmakers, DNA damage and ageing: new-age ideas for an age-old problem, Nat. Cell Biol. 10 (2008) 1241–1247.
[89] M. Lebel, R.D. Cardiff, P. Leder, Tumorigenic effect of nonfunctional p53 or p21 in mice mutant in the Werner syndrome helicase, Cancer Res. 61 (2001) 1816–1819.
[90] M. Lebel, J. Lavoie, I. Gaudreault, M. Bronsard, R. Drouin, Genetic cooperation between the Werner syndrome protein and poly(ADP-Ribose) polymerase-1 in preventing chromatid breaks, complex chromosomal rearrangements, and cancer in mice, Am. J. Pathol. 162 (2003) 1559–1569.
[91] R. Agrelo, W.H. Cheng, F. Setien, S. Ropero, J. Espada, M.F. Fraga, M. Herranz, M.F. Paz, M. Sanchez-Cespedes, M.J. Artiga, D. Guerrero, A. Castells, C. von Kobbe, V.A. Bohr, M. Esteller, Epigenetic inactivation of the premature aging Werner syndrome gene in human cancer, Proc. Natl. Acad. Sci. U.S.A. 103 (2006) 8822–8827.
[92] P.L. Opresko, J.P. Calvo, C. von Kobbe, Role for the Werner syndrome protein in the promotion of tumor cell growth, Mech. Ageing Dev. 128 (2007) 423–436.
[93] T. Kawasaki, M. Ohnishi, Y. Suemoto, G.J. Kirkner, Z. Liu, H. Yamamoto, M. Loda, C.S. Fuchs, S. Ogino, WRN promoter methylation possibly connects mucinous differentiation, microsatellite instability and CpG island methylator phenotype in colorectal cancer, Mod. Pathol. 21 (2007) 150–158.